Supporting Information for

Mediator-assisted synthesis of WS2 with ultrahigh-optoelectronic performance at multi-wafer scale

Yu-Siang Chen[1], Sheng-Kuei Chiu[2], De-Liang Tsai[3], Chong-Yo Liu[4], Hsiang-An Ting[5], Yu-Chi Yao[4], Hyungbin Son[6], Golam Haider[7], Martin Kalbáč[7], Chu-Chi Ting[3], Yang-Fang Chen[4], Mario Hofmann[4], Ya-Ping Hsieh[*]

[1] Institute of Atomic and Molecular Sciences, Academia Sinica. Taipei, Taiwan 10617

[2] Department of Material Science and Engineering, Feng Chia University, Taichung, Taiwan 40724

[3] Graduate Institute of Opto-Mechatronics, Department of Mechanical Engineering, National Chung Cheng University, Chia-Yi, Taiwan, 62102

[4] Department of Physics, National Taiwan University, Taipei, Taiwan 10617

[5] Department of Mechanical Engineering, National Chiao Tung University, Hsinchu, Taiwan, 30010

[6] Department of Integrative Engineering, Chung Ang University, Seoul, Republic of Korea, 06974

[7] J. Heyrovsky Institute of Physical Chemistry of the Czech Academy of Sciences, Dolejškova 2155/3, 182 23, Prague, Czech Republic

Corresponding author. Email: yphsieh@gate.sinica.edu.tw

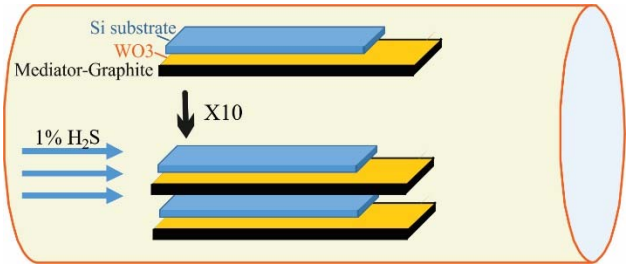

Supplementary Figure 1. Illustration of stacked mediator-assisted growth method.

Supplementary Note 1

Graphene-based mediator

In addition to graphite, graphene was employed as a mediator. Raman characterization indicated that for reaction times over 30 minutes the graphene mediator disappeared, which indicates that mediators are consumed at a rate of approximately 10^{12} s^{-1}. This disappearance agrees with thermochemical calculations that indicate the conversion to gaseous carbon oxides.

Supplementary Note 2

Comparison of WS_2 from different sources:

Optical micrographs show that conventional CVD and exfoliation produce individual grains with micrometer size whereas mediator-grown WS_2 demonstrates uniform coverage.

Raman spectroscopy of all materials was conducted in a confocal system with 532nm excitation and WS_2 from all three sources show the characteristic A_{1g} and E_{2g} vibration modes. Compared to exfoliated WS_2, the A_{1g} (at 417.6 cm^{-1}) of mediator-grown WS_2 remained at the position while the E_{2g} (at 349.3 cm^{-1}) is slight red-shifted. This behavior has been previously reported to be due to tensile strain[1].

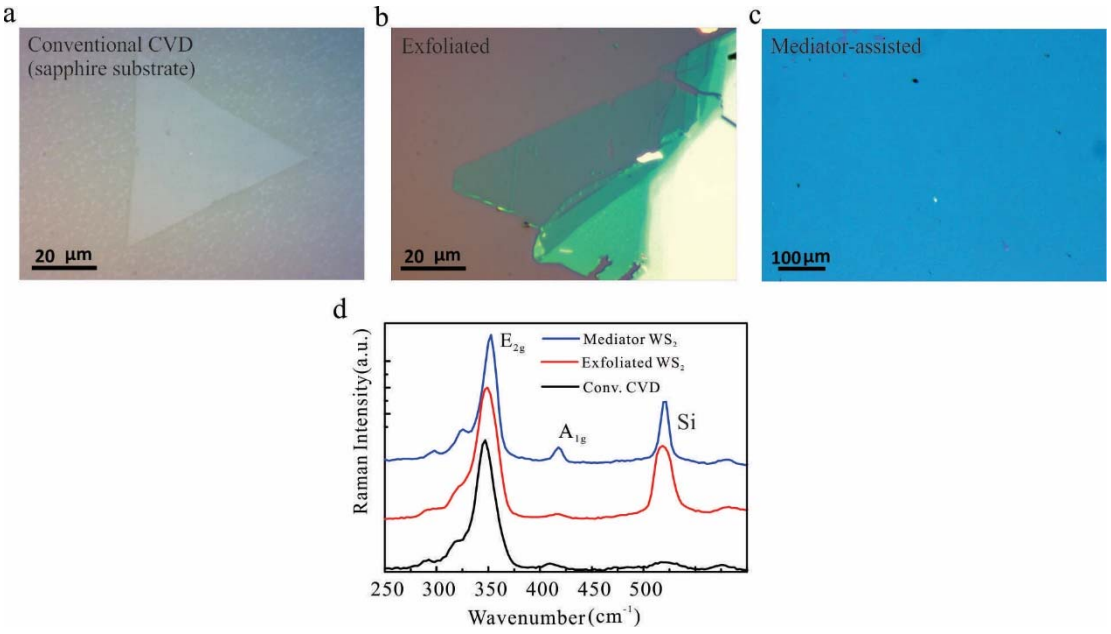

Supplementary Figure 2. Comparison of WS_2 from various sources. Raman and OM images for conventional, exfoliated and mediator-assisted WS_2. Investigation of lattice defects

Supplementary Note 3

Estimation of defect density from HR-TEM

We investigated large arrays of HRTEM images to identify defects and found that the prevalent type of defect are multi-atom vacancies and tears. This defect type is different from previous reports which observed predominant vacancy-type defects. We therefore hypothesize that these large defects are induced during transfer from the growth substrate to the TEM grid.

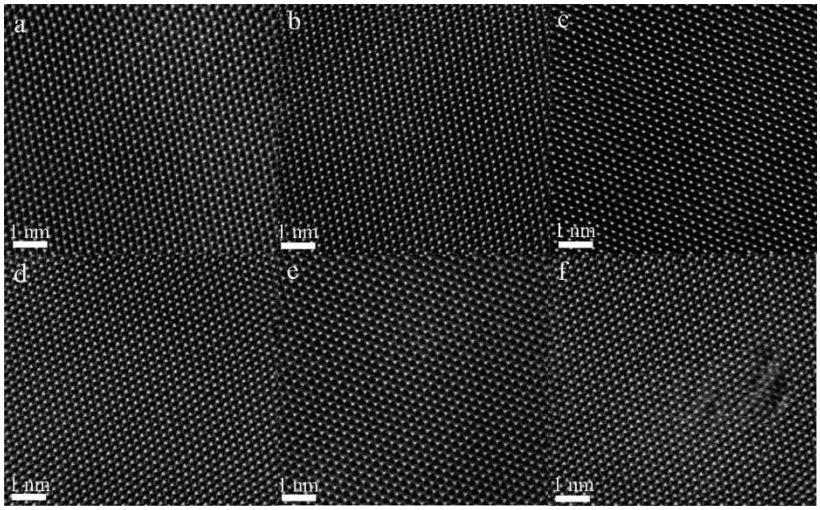

Supplementary Figure 3. Visualizing defects. Composite picture of 6 HRTEM images with indication of multi-atom defect.

Supplementary Note 4

Calculation of Fermi level:

The intrinsic Fermi level can be calculated according to

$$E_{\mathrm{F}} = \frac{E_{\mathrm{gap}}}{2} + \frac{kT}{2}\ln\left(\frac{D_{\mathrm{V}}}{D_{\mathrm{C}}}\right) \quad (1)$$

, where $D_{v,c}$ are the edge densities of states for the valence and conduction band, respectively

$$D_{\mathrm{v,c}} = m_{\mathrm{h,e}}{}^{*}/\pi\hbar^{2} \quad (2)$$

, here m* is the effective mass of holes and electrons, respectively. Theoretical work has estimated the effective masses in WS_2 to be $0.37m_e$ and $0.38m_e$ for holes and electrons, respectively[2]. Comparison of the intrinsic and measured Fermi level suggests an extrinsic doping density of $3 \times 10^{12}\mathrm{cm}^{-2}$ but this value is associated with a large error due to the absence of experimental values for the effective mass of WS_2.

Supplementary Note 5

Spectroscopic characterization of sample uniformity:

We have conducted large-scale optical spectroscopic characterization to establish the uniformity of mediator-grown material. For this purpose, 10,000 photoluminescence (PL) and Raman spectra taken from a 7x2cm sample size and individually fit to Lorentzian peaks using a MATLAB fitting routine. Histograms of the PL peak intensities demonstrate a narrow distribution compared to the wide spread of intensities observed in CVD grown WS_2. This observation indicates the lower variability of emission properties in mediator-assisted growth. Moreover, the PL peak position of mediator-assisted growth corresponds exclusively to the neutral exciton energy whereas CVD-grown WS_2 exhibits a large contribution of defect-related biexcitons, suggesting the presence of alternative recombination pathways. Finally, statistical analysis of the separation between the E_{2g} and A_{1g} Raman peaks indicates that mediator grown material is exclusively composed of single-layers[3].

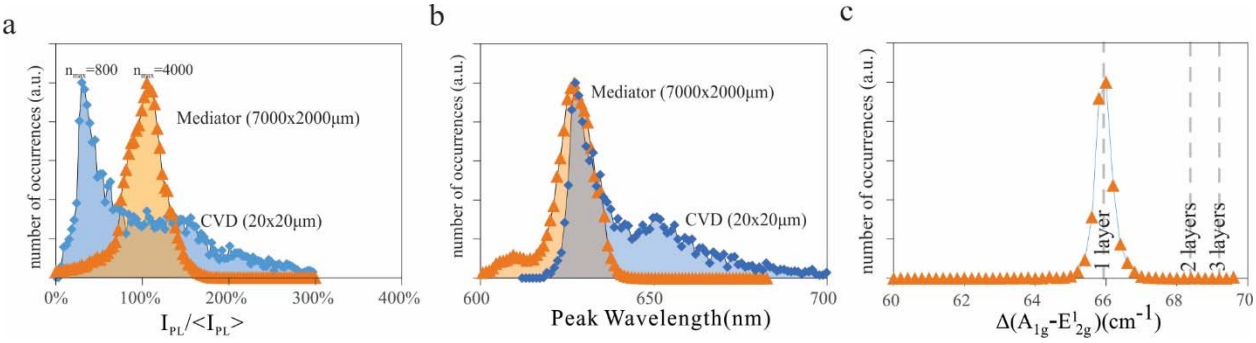

Supplementary Figure 4. Statistical analysis for CVD grown and mediator-grown WS_2 at indicated dimensions (a) scaled histogram of photoluminescence intensity normalized to average intensity,**(b)** histogram of photoluminescence wavelength of the strongest peak in each PL spectrum, **(c)** histogram of energy difference between Raman E_{2g} and A_{1g} features.

Supplementary Note 6

Photoelectron spectroscopy

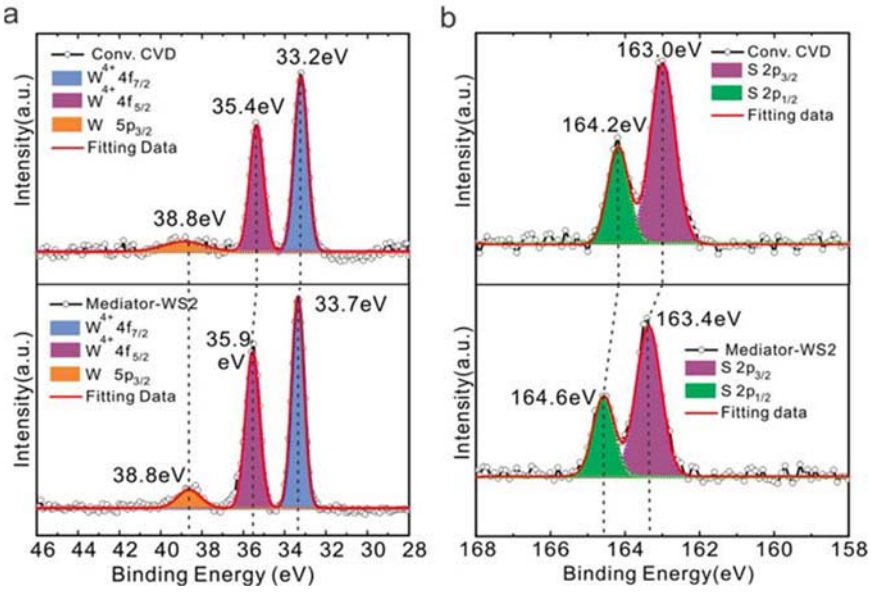

Supplementary Figure 5. XPS of conventional CVD v.s Mediator-assisted grown WS_2.

The observation of tensile strain is supported by X-ray photoelectron spectroscopy which shows the S $2p_{1/2}$ and S $2p_{3/2}$ peaks located at around 163.0eV and 164.2eV and the $W^{4+}4f_{5/2}$ and $4f_{7/2}$ peaks at 35.4eV and 33.2eV, respectively.[4]Both peaks exhibit a significant blueshift which has been attributed to the occurrence of strain in WS_2 monolayers[5].

Ambient Photoelectron spectroscopy was conducted in a APS01 system (KP Technology Ltd), Figure 3(d) shows an exponential tail close to the conduction band edge that has been previously observed for WS_2 and MoS_2 by electrical measurements[6].

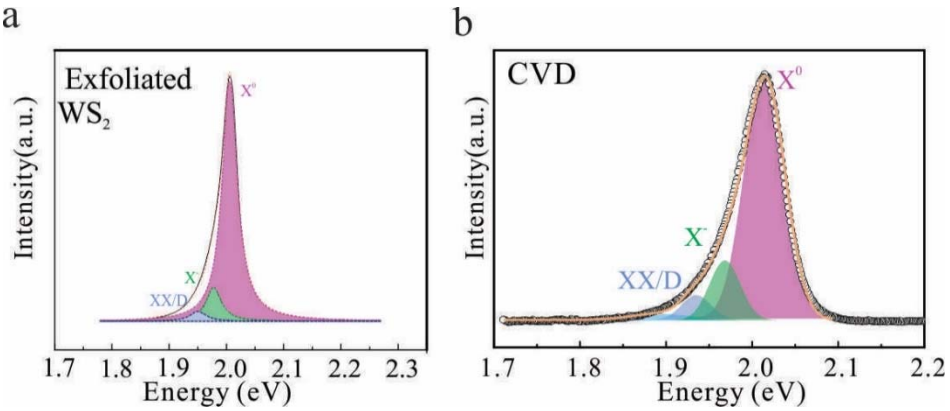

Supplementary Figure 6. Fitting of WS_2 PL spectra from different sources.

The PL spectrum for each WS_2 source is deconvoluted into peaks corresponding to different contributions. Following previous reports[7], we assign the following excitonic transitions from high to lower energy: Neutral (X^0, 2.01 eV) , Trion (X^-, 1.96eV), defect-bound exciton (*XX*/*D*, 1.94 eV).

Supplementary Note 7

Details on photosensor characterization:

The photoresponse time was extracted by fitting the photocurrent under pulsed illumination to the formula

$$i = i_0\left(1 - e^{-\frac{t}{\tau}}\right) \quad (3)$$

The resulting time constant is extracted to be $r = 58\mu s$

The responsivity was calculated according to

$$R = \frac{i_\mathrm{p}}{P} \quad (4)$$

, where i_p is the photocurrent (I_{light}-I_{dark}) and P is the incident light power.

The detectivity D* in the shot-noise limit is calculated according to

$$D^* = RA^{\frac{1}{2}}(2qI_\mathrm{dark})^{-1/2} \quad (5)$$

,where A is the device area.

Under 1.4 μW/cm2 excitation, the measured dark current at 15V is 0.98×10^{-6} A, and the on current is 8.05×10^{-6} A. Considering a channel area of ~2×10^{-4} cm^2, we obtain a maximum photoresponse of ~25000 A/W.

The photoresponse time was measured under pulsed white light excitation with power of 30 μW cm^-2 using a SR-540 optical chopper. Each device had dimensions of 400μm(W) x 50μm(L).

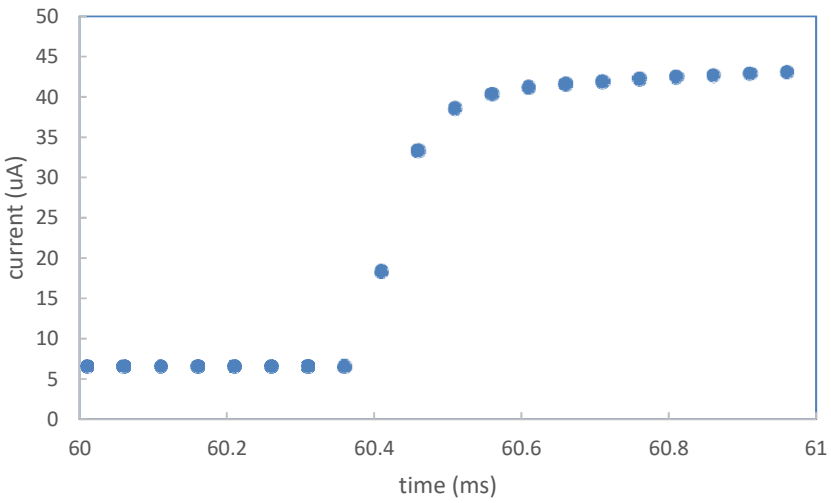

Supplementary Figure 7. High-speed response. Current response under pulsed light illumination (intensity of 30 µW cm^-2) indicating high-speed response in with fit.

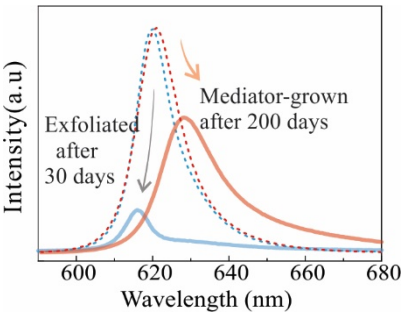

Supplementary Figure 8. Stability test. Photoluminescence spectra of exfoliated and mediator-grown WS_2 after different duration of exposure to ambient environment.

Supplementary Table 1. Comparison of photosensor performance to previous reports.

Material	Method	Response time(s)	Responsivity(A/W)	Reference
Multilayer WS_2	CVD	5.30E-03	9.20E-05	[8]
Monolayer WS_2	CVD	6.00E-02	1.88E-02	[9]
WS_2	CVD	9.10E+01	9.50E+02	[10]
Multilayer WS_2	mechanical exfoliation	2.00E-02	5.70E+00	[11]
few layer WS_2	Li-ion intercalation technique	4.20E-02	1.10E+00	[12]
multilayered WS_2	pulsed-laser deposition	4.10E+00	5.10E-01	[13]
WS_2	exfoliated	7.90E+00	4.04E+00	[14]
Monolayer WS_2	CVD	5.60E-04	5.20E-04	[15]
Single-Layer WS_2	CVD	2.00E-03	4.50E+03	[12]
This work	**Mediator-assisted CVD**	**5.80E-05**	**2.50E+04**	

Supplementary References

1. McCreary KM, Hanbicki AT, Singh S, Kawakami RK, Jernigan GG, Ishigami M*, et al.* The Effect of Preparation Conditions on Raman and Photoluminescence of Monolayer WS2. *Scientific Reports* 2016, **6**(1)**:** 35154.

2. Zhang C, Gong C, Nie Y, Min K-A, Liang C, Oh YJ*, et al.* Systematic study of electronic structure and band alignment of monolayer transition metal dichalcogenides in Van der Waals heterostructures. *2D Materials* 2016, **4**(1)**:** 015026.

3. Li Y, Li X, Yu T, Yang G, Chen H, Zhang C*, et al.* Accurate identification of layer number for few-layer WS2 and WSe2 via spectroscopic study. *Nanotechnology* 2018, **29**(12)**:** 124001.

4. Yao H, Liu L, Wang Z, Li H, Chen L, Pam ME*, et al.* Significant photoluminescence enhancement in WS2 monolayers through Na2S treatment. *Nanoscale* 2018, **10**(13)**:** 6105-6112.

5. Desai SB, Seol G, Kang JS, Fang H, Battaglia C, Kapadia R*, et al.* Strain-Induced Indirect to Direct Bandgap Transition in Multilayer WSe2. *Nano Letters* 2014, **14**(8)**:** 4592-4597.

6. Ovchinnikov D, Allain A, Huang Y-S, Dumcenco D, Kis A. Electrical Transport Properties of Single-Layer WS2. *ACS Nano* 2014, **8**(8)**:** 8174-8181.

7. Cong C, Shang J, Wang Y, Yu T. Optical Properties of 2D Semiconductor WS2. *Advanced Optical Materials* 2018, **6**(1)**:** 1700767.

8. Perea-López N, Elías AL, Berkdemir A, Castro-Beltran A, Gutiérrez HR, Feng S*, et al.* Photosensor Device Based on Few-Layered WS2 Films. *Advanced Functional Materials* 2013, **23**(44)**:** 5511-5517.

9. Lan C, Li C, Yin Y, Liu Y. Large-area synthesis of monolayer WS2 and its ambient-sensitive photo-detecting performance. *Nanoscale* 2015, **7**(14)**:** 5974-5980.

10. Lan C, Li C, Wang S, He T, Zhou Z, Wei D*, et al.* Highly responsive and broadband photodetectors based on WS2–graphene van der Waals epitaxial heterostructures. *Journal of Materials Chemistry C* 2017, **5**(6)**:** 1494-1500.

11. Huo N, Yang S, Wei Z, Li SS, Xia JB, Li J. Photoresponsive and gas sensing field-effect transistors based on multilayer WS_2 nanoflakes. *Sci Rep* 2014, **4:** 5209.

12. Aji AS, Solís-Fernández P, Ji HG, Fukuda K, Ago H. High Mobility WS2 Transistors Realized by Multilayer Graphene Electrodes and Application to High Responsivity Flexible Photodetectors. *Advanced Functional Materials* 2017, **27**(47)**:** 1703448.

13. Yao JD, Zheng ZQ, Shao JM, Yang GW. Stable, highly-responsive and broadband photodetection based on large-area multilayered WS2 films grown by pulsed-laser deposition. *Nanoscale* 2015, **7**(36)**:** 14974-14981.

14. Li J, Han J, Li H, Fan X, Huang K. Large-area, flexible broadband photodetector based on WS2 nanosheets films. *Materials Science in Semiconductor Processing* 2020, **107:** 104804.

15. Lan C, Zhou Z, Zhou Z, Li C, Shu L, Shen L*, et al.* Wafer-scale synthesis of monolayer WS2 for high-performance flexible photodetectors by enhanced chemical vapor deposition. *Nano Research* 2018, **11**(6)**:** 3371-3384.